electronics

MDPI

Article

Joint Jamming Avoidance and Suppression with Intelligent Detection Threshold Adaptation for Emergency Wireless Communications

Zhiyu Li [1,2,3], Lulu Zhang [4], Xiaoyang Wang [1,2,3], Lili Hu [1,2,3], Zhilei Zhang [4], Cheng Zhang [4,5,†] and Changwei Zhang [4,*,†]

[1] CRSC Low-Altitude Intelligence Technology Co., Ltd., Beijing 100070, China; lizhiyu@crsc.cn (Z.L.); wangxiaoyang@crsc.cn (X.W.); hulili@crsc.cn (L.H.)
[2] National Railway Administration Innovation Base of Low-Altitude Applications and Safety (Engineering Research Center), Beijing 100070, China
[3] Beijing Key Laboratory of Intelligent Management and Control of Low-Altitude Airspace, Beijing 100070, China
[4] Pervasive Communication Research Center, Purple Mountain Laboratories, Nanjing 211111, China; zhanglulu@pmlabs.com.cn (L.Z.); zhangzhilei@pmlabs.com.cn (Z.Z.); zhangcheng_seu@seu.edu.cn (C.Z.)
[5] National Mobile Communications Research Laboratory, Southeast University, Nanjing 211111, China
* Correspondence: zhangchangwei@pmlabs.com.cn
† Cheng Zhang and Changwei Zhang are Members, IEEE.

Abstract

As wireless communication technologies continue to evolve, malicious jamming becomes a major factor that limits system performance and communication quality, especially in emergency communication scenarios where reliable links are essential for timely information delivery and rescue coordination. Conventional anti-jamming transmission methods often suffer from two issues. In the detection stage, the jamming threshold is difficult to determine. In the data transmission stage, spectrum resources are not efficiently utilized. To address these limitations, this paper jointly considers jamming detection and data transmission, and proposes a joint jamming avoidance and suppression method based on intelligent detection threshold adaptation. Specifically, reinforcement learning is first used to iteratively optimize the detection threshold according to transmission outcomes, which improves the accuracy and robustness of jamming detection. Then, based on the detection results, the jamming status is dynamically evaluated, then jamming avoidance and jamming suppression are jointly employed during data transmission, which effectively improves spectrum utilization. Simulation results show that, under both continuous-band jamming and comb-spectrum jamming, the proposed scheme nearly doubles the system sum rate and also achieves significantly higher detection accuracy than conventional methods, which demonstrates strong robustness and adaptability for emergency communication systems.

Keywords: wireless communications; anti-jamming; jamming detection; jamming avoidance and suppression

Check for updates

Academic Editor: Stefano Scanzio

Received: 28 September 2026
Revised: 23 October 2026
Accepted: 28 October 2026
Published: 3 November 2026

Copyright: © 2026 by the authors. Licensee MDPI, Basel, Switzerland. This article is an open access article distributed under the terms and conditions of the Creative Commons Attribution (CC BY) license.

1. Introduction

The rapid advancement of fifth-generation (5G) and sixth-generation (6G) mobile communication technologies has brought remarkable improvements in spectrum efficiency, transmission rate, and connection density [1–3]. However, the increasingly complex electromagnetic environment has made malicious jamming a critical challenge that threatens

communication reliability, particularly in emergency communication scenarios where network infrastructure may be damaged and communication resources are highly constrained. In such scenarios, jamming signals can severely damage legitimate communication links through temporal, spectral, or spatial domains, leading to increased bit error rates (BERs), degraded throughput, or even complete communication interruption [4–6]. Consequently, efficient and intelligent anti-jamming techniques for wireless communications have become a prominent research focus in both academia and industry.

Anti-jamming technology primarily consists of two components: jamming detection and anti-jamming data transmission. During the detection phase, the jamming information must be accurately identified to provide decision-making foundations for subsequent anti-jamming transmission. Generally speaking, jamming detection mainly includes signal energy-based methods and feature-based methods [7]. As a typical energy detection algorithm, the forward consecutive mean excision (FCME) algorithm determines appropriate detection thresholds by calculating signal means [8]. Zhou et al. proposed using bispectral transformation for feature extraction and designed a feature fusion algorithm based on Bayesian decision theory to identify jamming signals with high precision [9]. However, these methods often require manual configuration of certain detection parameters and cannot adapt to dynamic changes in jamming power [10–12]. To address these limitations, reinforcement learning (RL) has gradually emerged as a research hotspot due to its online learning and dynamic decision-making capabilities. For instance, Wang et al. applied Q-learning to spectrum sensing in cognitive radio, improving jamming detection accuracy and speed by optimizing detection thresholds and frequency band numbers [13]. Nevertheless, such purely data-driven approaches may suffer from limited interpretability and uncontrollable outputs.

Anti-jamming transmission techniques are mainly categorized into jamming avoidance and jamming suppression. Specifically, jamming avoidance dynamically adjusts transmission parameters such as frequency and time slots to evade jamming signals, with representative methods including dynamic spectrum access in cognitive radio [14–16] and frequency hopping techniques [17–19]. For example, Qi et al. proposed a game-theoretic spectrum allocation algorithm to minimize interference experienced by legitimate users [15]. Atheeq et al. utilized the unpredictability and randomness of chaotic mappings to design secure frequency hopping sequences to reduce the probability of being jammed [17]. However, these methods perform well under narrowband or wideband jamming scenarios but often struggle to find continuous time-frequency resource blocks (RBs) unaffected by jamming when facing comb-spectrum interference, leading to degraded anti-jamming performance [20,21].

Jamming suppression techniques focus on eliminating existing interference through signal processing, with typical methods including pulse clipping [22,23] and adaptive filtering based on precoding [24–26]. Shhab et al. investigated the use of clipping and blanking preprocessing filters to suppress impulsive noise effects in millimeter-wave communication systems, demonstrating through extensive simulations that selecting optimal thresholds is crucial for reducing impulsive noise components [23]. Although pulse clipping can effectively suppress jamming effects, it simultaneously suppresses normal data symbols during the clipping process, preventing the application of high-order modulation and reducing communication efficiency. Regarding adaptive filtering, Wang et al. optimized beamforming weights to place nulls in jamming directions, significantly improving the jamming-to-signal ratio (JSR) resistance [26]. In recent years, researchers have introduced machine learning into the jamming suppression domain [27,28]. For example, Hao et al. proposed an adaptive anti-jamming beamforming method based on preprocessing deep RL, which eliminates wavefront distortion under dynamic jamming through convolu-

tional neural network preprocessing and RL strategies, significantly improving system sum rates [27].

To address these challenges, this paper proposes a joint jamming avoidance and suppression (JJAS) method based on intelligent detection threshold adaptation. Compared with FCME using a fixed threshold factor, our detector adjusts this factor using sum rate and BER feedback. The learning action is the FCME threshold factor, and the reward reflects transmission performance. The detected frequency points also support interference-plus-noise (IPN) estimation and Type 0 resource block group (RBG) allocation. In addition to selecting frequency resources, the transmission stage suppresses detected jammed subcarriers and selects modulation and coding schemes (MCSs). Compared with the Q-learning detector of Wang et al., which adjusts the detection threshold and the number of power spectral density (PSD) bins to improve detection speed and accuracy [13], our method retains the FCME procedure and uses sum rate and BER feedback to select its threshold factor. The detected frequency points also support IPN estimation and resource allocation. Compared with dynamic spectrum access, the transmission strategy includes suppression of detected jammed subcarriers and Type 0 RBG allocation with MCS selection. Compared with RL beamforming [27], the control variables concern the detection threshold and frequency resources rather than beamforming weights. The main contributions are summarized as follows.

First, we develop an adaptive jamming detector that combines the FCME procedure with online Q-learning. A Markov decision process uses sum rate and BER feedback to describe the transmission state, while the learning action selects the FCME threshold factor. The reward accounts for rate changes and a BER penalty, so threshold selection is guided by transmission performance. This design retains the FCME detection procedure while allowing its threshold to adapt to changes in jamming conditions.

Second, we develop a JJAS transmission strategy that connects the detected frequency points with IPN estimation, subcarrier suppression, and Type 0 RBG allocation with MCS selection. Given jamming-type information from a recognition module, the strategy combines avoidance and suppression for continuous-band jamming and uses suppression for comb-spectrum jamming. Suppression operates on detected jammed subcarriers, while resource allocation operates on RBGs. This allows an affected RBG to remain available for transmission using its remaining received information and a suitable MCS.

Third, we evaluate the method in a Sub-6G orthogonal frequency division multiplexing (OFDM) uplink under continuous-band and comb-spectrum jamming. The detection results illustrate initial learning and adaptation after a change in jamming strength within one continuous run. The transmission results compare JJAS with conventional Type 0 allocation under the same system and jamming settings. In the tested scenarios, JJAS nearly doubles the system sum rate. Under comb-spectrum jamming, the worst-user rate remains around 10 Mbps, showing improved service to the most affected user compared with the baseline.

The rest of this paper is organized as follows. Section 2 presents the system model and analyzes the effect of jamming. Section 3 introduces the intelligent FCME-based jamming detection method. Section 4 presents the proposed joint jamming avoidance and suppression transmission strategy. Section 5 provides simulation results. Section 6 concludes this paper.

2. System Model

2.1. Basic Link for Anti-Jamming Wireless Data Transmission

Figure 1 illustrates the basic link of the anti-jamming OFDM system. At the transmitter, source bit data first undergoes encoding, interleaving, and constellation modulation, then serial-to-parallel conversion for OFDM modulation, followed by adding cyclic prefixes. Finally, the signal is sent to the channel, and the transmitted signal superimposed with noise

and jamming signals arrives at the receiver. At the receiver, the received signal undergoes OFDM demodulation, and the intelligent FCME jamming detection algorithm detects the jamming signal residence frequency band. Based on jamming detection results, the OFDM system transmitter and receiver dynamically adjust time-frequency resources used in the next time slot. Meanwhile, a channel gain maximization-based combinatorial optimization problem is designed using data channel gains on different frequency bands, and solving this problem achieves optimal resource scheduling. Then, jamming suppression is performed at the receiver to filter out jamming signals. Subsequently, channel estimation and noise estimation are conducted, and the results are sent to the soft decision module to obtain soft information of coded bits, which are then deinterleaved and decoded.

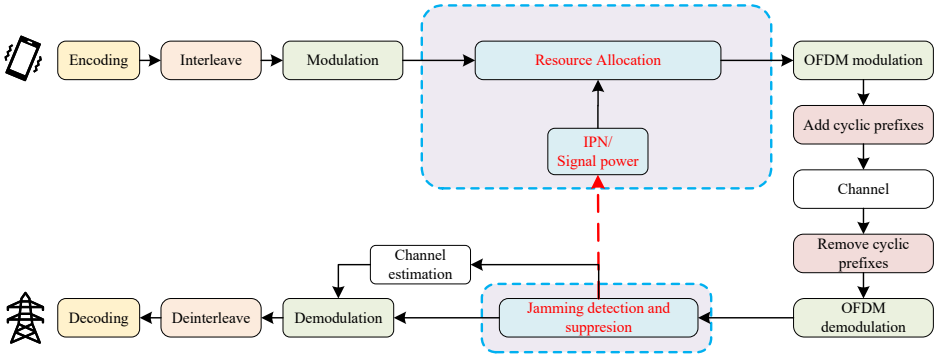


Figure 1. Basic link for the anti-jamming wireless data transmission.

In this paper, wireless transmission resource allocation adopts the Type 0 allocation method [29], i.e., combining multiple consecutive RBs into an RBG, and allocating resources to users in units of RBG. The base station determines RBG size and total number based on system bandwidth and other configuration information, and determines RBG sets allocated to users based on user resource requirements, channel conditions, and other factors.

2.2. Received Signal Model

We use a subcarrier-level received signal model to describe the effects of the wireless channel and jamming on OFDM transmission. The received signal contains the desired signal after channel propagation, the jamming signal, and noise. Let x_k denote the transmitted symbol on subcarrier k, so the received signal y_k is expressed as

$$y_k = h_k x_k + j_k + n_k, \tag{1}$$

where h_k represents the channel impulse response on subcarrier k, j_k denotes the jamming signal, and n_k represents additive white Gaussian noise.

In practical applications, wireless channels typically exhibit time-varying and frequency-selective characteristics, which significantly affect received signals. Multipath propagation causes signal delay spread and frequency-selective fading, while the presence of jamming signals further degrades system performance. Therefore, accurate modeling of wireless channels is essential for anti-jamming technique design.

2.3. Channel Estimation Method

Channel estimation provides the channel gains needed for signal detection and resource allocation. Known pilot symbols are used to estimate these gains at pilot positions. We first consider transmission without jamming, where the received signal on pilot subcarrier p is expressed as

$$y_p = h_p x_p + n_p, \tag{2}$$

where x_p is the pilot symbol on the p-th pilot subcarrier. The channel gain can be estimated using the least squares (LS) method:

$$\hat{h}_p = \frac{y_p}{x_p}. \tag{3}$$

Pilots occupy selected subcarriers in selected OFDM symbols, so channel estimates obtained directly from pilots do not cover all data positions. Interpolation uses these pilot estimates to obtain channel gains at positions without pilots. The resulting channel estimates are then used for data detection and recovery.

Common channel estimation methods include linear interpolation and minimum mean square error (MMSE) interpolation. Linear interpolation estimates the channel gain at a data position as a weighted sum of neighboring pilot estimates. The weights depend on the distance between the data position and each pilot position. This method is simple to implement, and the estimate is expressed as

$$\hat{h}_d = \frac{d - p_1}{p_2 - p_1}\hat{h}_{p_2} + \frac{p_2 - d}{p_2 - p_1}\hat{h}_{p_1}, \tag{4}$$

where $\hat{h}_d$ is the channel estimation value corresponding to the d-th target data position, and $\hat{h}_{p_1}$ and $\hat{h}_{p_2}$ are channel estimation values at the p_1-th and p_2-th pilot positions.

MMSE interpolation uses the correlation between channel gains at pilot and data positions to determine the interpolation weights. These weights are chosen to minimize the mean squared error between the true and estimated channel gains. The error is defined as

$$\epsilon = \mathbb{E}[|\mathbf{h}_d - \hat{\mathbf{h}}_d|^2]. \tag{5}$$

By minimizing this error, the channel estimates at data positions are obtained from the pilot estimates and the channel correlation matrices as

$$\hat{\mathbf{h}}_d = \mathbf{R}_{dp}\mathbf{R}_{pp}^{-1}\hat{\mathbf{h}}_p, \tag{6}$$

where $\mathbf{R}_{dp}$ is the cross-correlation matrix between targets and pilots, $\mathbf{R}_{pp}$ is the auto-correlation matrix of pilot channel gains, and $\hat{\mathbf{h}}_p$ represents channel estimation values at all pilot subcarrier positions.

From the above analysis, jamming affects channel estimation in two main aspects. First, when the pilot signal on the p-th subcarrier is jammed, the LS channel estimation becomes

$$\hat{h}_p = \frac{h_p x_p + j_p + n_p}{x_p} = h_p + \frac{j_p}{x_p} + \frac{n_p}{x_p}. \tag{7}$$

The term j_p/x_p affects the pilot estimate even when noise is small. Interpolation spreads this error to the channel estimates at data positions, extending the effect of jamming beyond the jammed pilots.

2.4. Common Jamming Types and Impact Analysis

In wireless communications, common jamming types include continuous band jamming and comb-spectrum jamming. Specifically, continuous band jamming can be generated by passing white Gaussian noise through a narrowband filter, with the filter frequency response $H(f)$

$$H(f) = \begin{cases} 1, & |f - f_j| \le \frac{B_j}{2} \\ 0, & \text{otherwise}, \end{cases} \tag{8}$$

where f_j represents the jamming signal center frequency and B_j represents the jamming bandwidth. This paper defines narrowband jamming when B_j is less than 20% of the

communication bandwidth, and wideband jamming when exceeding 20% of the communication bandwidth. Single-tone jamming can be viewed as a special case when B_j equals one subcarrier bandwidth.

Comb-spectrum jamming can be viewed as composed of multiple continuous band jamming segments, with the filter frequency response

$$H(f) = \sum_{i=1}^{N_c} \begin{cases} 1, & |f - f_{j,i}| \leq \frac{B_{j,i}}{2} \\ 0, & \text{otherwise,} \end{cases} \tag{9}$$

where $f_{j,i}$ represents the center frequency of the i-th continuous band jamming signal, $B_{j,i}$ represents the bandwidth of the i-th continuous band jamming signal, and N_c is the number of comb-spectrum components. Multi-tone jamming can be viewed as a special case when $B_{j,i}$ equals one subcarrier bandwidth.

Under continuous-band jamming, the system can avoid the affected band and allocate resources in the remaining spectrum when sufficient resources are available. Under comb-spectrum jamming, the unjammed gaps between adjacent jamming components may be narrower than an RBG. Resource allocation alone may therefore be unable to avoid all jammed subcarriers. To address these different conditions, the proposed transmission strategy combines avoidance and suppression for continuous-band jamming and uses suppression of detected jammed subcarriers for comb-spectrum jamming.

3. Intelligent FCME-Based Jamming Detection Method

Accurate jamming detection provides the information needed for subsequent anti-jamming transmission. This section presents an FCME detector with an adaptive threshold selected using transmission feedback.

3.1. Basic Principles

Threshold detection is used to detect jamming and identify its frequency distribution. The FCME algorithm first sorts the frequency points by signal power. The lowest 10% form the initial unjammed set, with at least one point included. The remaining points form the candidate set. In each iteration, the threshold is calculated from the mean power of the unjammed set. Each candidate point is checked once against this threshold. Points with power at or below the threshold are added to the unjammed set and removed from the candidate set. The mean power and threshold are updated in the next iteration. The procedure stops when no new points can be added or the candidate set is empty. The remaining candidate points are identified as jammed. Algorithm 1 gives the detailed detection procedure.

It can be found that the jamming threshold is an important parameter of the FCME algorithm, which is obtained by multiplying the mean power of the current unjammed set by the adjustable factor η and the fixed coefficient $2\sqrt{-\ln(10^{-11})/\pi}$. The reference false-alarm parameter 10^{-11} sets this coefficient, which is approximately 5.68. Current FCME-based jamming detection algorithms require removal of useful signal effects (retaining only noise and possible jamming) to accurately determine jamming thresholds, which is difficult to achieve in practical systems. Furthermore, in complex and variable channel environments, this method often fails to achieve expected results, leading to low jamming detection accuracy. Therefore, how to efficiently and accurately determine the optimal jamming threshold is a key technical challenge in current jamming detection and suppression.

Algorithm 1 FCME jamming detection algorithm

Input Signal power $\{P_k\}_{k=1}^{N}$, number of frequency points N, threshold factor η
Output Jammed frequency-point set S_j

Sort the original indices so that $P_{\pi_1} \le \cdots \le P_{\pi_N}$
$N_0 = \max\{1, \lceil 0.1N \rceil\}$
$S_n = \{\pi_1, \ldots, \pi_{N_0}\}$
$S_c = \{1, \ldots, N\} \setminus S_n$
while $S_c \neq \emptyset$ **do**
    $P_n = \frac{1}{|S_n|} \sum_{k \in S_n} P_k, \quad T = \eta P_n 2\sqrt{-\ln(10^{-11})/\pi}$
    $S_{\text{add}} = \emptyset$
    for each $k \in S_c$ **do**
        if $P_k \le T$ **then**
            $S_{\text{add}} = S_{\text{add}} \cup \{k\}$
        end if
    end for
    if $S_{\text{add}} = \emptyset$ **then**
        break
    end if
    $S_n = S_n \cup S_{\text{add}}$
    $S_c = S_c \setminus S_{\text{add}}$
end while
$S_j = S_c$

Generally speaking, the determination of jamming thresholds can be viewed as a Markov decision process, and RL is a powerful method for solving Markov decision problems. By introducing RL, the threshold can be optimized through interaction with the environment and continuous trial and error. Specifically, the signal receiver is regarded as an agent, which discriminates between normal and abnormal states based on received signal rates, BERs, and other states, selects and executes corresponding actions in the current state, acts on the current jamming detection environment, then analyzes the signal receiver state and provides corresponding reward or penalty feedback based on the state. Using reward or penalty mechanisms, the association between states and optimal decisions is strengthened. Through repeated iteration of this process, the model continuously learns and gradually acquires the ability to select optimal strategies.

3.2. Q-learning Model Parameter Definition

To accurately describe normal and abnormal states of jamming detection, the state space is defined as $\mathcal{S} = \{R, \text{BER}\}$, where R represents the sum rate and BER represents the user average BER. To enable rapid algorithm convergence and quick response to jamming environment changes, the state set is simplified.

Specifically, for user sum rates, specific sum rate values are not considered. Instead, sum rate levels are defined according to service requirements and experience, with three categories established. When sum rate $R < R_{\text{low}}$, it is classified as low sum rate category with state value $s_R = 1$. When sum rate range is $R_{\text{low}} \le R < R_{\text{high}}$, it is defined as medium sum rate category with state value $s_R = 2$. When $R \ge R_{\text{high}}$, it is classified as high sum rate category with state value $s_R = 3$, thereby closely associating sum rate states with application scenarios and quality of service requirements.

Similarly, continuous BERs are mapped to a discrete state space with three categories defined. When user average BER $<$ BER_{low}, it is classified as excellent category with BER state value $s_{\text{BER}} = 1$. When average BER range is $\text{BER}_{\text{low}} \leq \text{BER} < \text{BER}_{\text{high}}$, it is defined as a moderate category with BER state value $s_{\text{BER}} = 2$. When BER $\geq$ BER_{high}, it is classified as a severe category with BER state value $s_{\text{BER}} = 3$, avoiding precise processing of specific BER values. The new state space $\mathcal{S}$ is expressed as

$$\mathcal{S} = \{(s_R, s_{\text{BER}}) | s_R \in \{1, 2, 3\}, s_{\text{BER}} \in \{1, 2, 3\}\} \tag{10}$$

where s_R represents the sum rate state value and s_{BER} represents the average BER state value.

The threshold factor η controls the sensitivity of jamming detection. A smaller value lowers the threshold, so more frequency points are identified as jammed. This can help detect weak jamming but may increase false alarms. A larger value raises the threshold, so fewer points are identified as jammed, which may reduce false alarms but increase missed detections. Different threshold factors therefore provide different balances between these two types of error. To keep the Q table small, the action space is defined as $\mathcal{A} = \{0.2, 0.4, 0.6, 0.8, 1.0, 1.2, 1.4, 1.6, 1.8\}$. The learning process selects among these factors using transmission feedback.

The reward function is calculated based on system sum rate changes and BER indicators:

$$r = \begin{cases} \alpha \cdot \frac{R_t - R_{t-1}}{R_{t-1}}, & \text{BER}_t < \text{BER}_{\text{th}} \\ \alpha \cdot \frac{R_t - R_{t-1}}{R_{t-1}} - \beta \cdot \text{BER}_t, & \text{BER}_t \geq \text{BER}_{\text{th}} \end{cases} \tag{11}$$

where R_t is the current time slot sum rate and R_{t-1} is the previous time slot sum rate. BER_t is the current time slot BER and BER_{th} is the BER threshold. When the current time slot BER is below the BER threshold, a reward is generated. α is the sum rate reward weight coefficient, determined according to system sensitivity to sum rate changes and the relative importance of sum rate in overall performance evaluation. When system sum rate improves, the agent obtains rewards related to sum rate improvement magnitude and weight coefficient, thereby incentivizing the agent to implement actions that improve sum rates.

When the current time slot average BER exceeds the predetermined BER threshold, the penalty mechanism activates, where β is the BER penalty weight coefficient, reflecting the penalty strength on reward values when average BER exceeds the threshold. This penalty mechanism aims to drive the agent to avoid actions that may cause excessively high BERs, as high BERs severely affect system communication quality and reliability. This reward function guides the agent through continuous learning and trial to find optimal strategies that can improve sum rates while ensuring BERs remain within acceptable ranges in complex environments.

3.3. Q-Value Table Update

The agent selects actions according to the ϵ-greedy strategy, choosing actions randomly with probability ϵ and selecting actions with maximum Q-values in the Q-table with probability $1 - \epsilon$. The agent executes the selected action, observes environmental feedback (next state and reward), then updates the Q-value of the current state-action pair using the Q-learning update rule. The update formula is:

$$Q(s_t, a_t) \leftarrow Q(s_t, a_t) + \alpha_Q [r_t + \gamma \max_{a'} Q(s_{t+1}, a') - Q(s_t, a_t)] \tag{12}$$

where s_t represents the state at time t, and a_t, a' are actions selected from action space $\mathcal{A}$ in states s_t and s_{t+1}, respectively. s_{t+1} represents the new state at time $t+1$ after taking action a_t. α_Q is the learning rate. r_t represents immediate reward, i.e., immediate reward obtained after taking action a_t in state s_t and transitioning to state s_{t+1}. γ is the discount factor, used to measure the importance of future rewards relative to current rewards.

3.4. Wireless Transmission Process Parameter Calculation

Based on accurate detection of jammed subcarriers, the IPN power of each RB and received signal power of each user can be further calculated for subsequent time-frequency resource allocation. Specifically, to calculate IPN, the received power on RBs without data transmission and unjammed can be averaged to obtain noise power σ_n^2. Since noise power changes slowly, σ_n^2 can also be measured before communication. On this basis, the average received power on RBs with data transmission and unjammed is calculated as signal plus noise (SPN) power P_{SPN}. Therefore, the IPN calculation formula on the m-th RB can be expressed as

$$P_{\text{IPN},m} = P_m - P_{\text{SPN}} + \sigma_n^2 \tag{13}$$

where P_m represents the received power on the m-th RB. User u's received signal power P_u can be expressed as:

$$P_u = \frac{1}{|\mathcal{M}_u|} \sum_{m \in \mathcal{M}_u} (P_{\text{SPN},m} - \sigma_n^2) \tag{14}$$

where set $\mathcal{M}_u$ represents the RB index collection occupied by user u.

The intelligent FCME-based jamming detection method described in this section achieves optimal jamming detection performance through adaptive optimization of the jamming threshold factor. In practical systems, due to jamming effects on channel estimation, accurately estimating IPN is difficult. To address this problem, in this paper, through the FCME-based jamming detection algorithm, the jamming frequency point can be identified precisely, IPN on each RB and user received signal power can thus be accurately calculated. These key parameters provide important input data for the time-frequency domain jamming avoidance and suppression methods in subsequent sections, laying a solid foundation for system anti-jamming performance optimization in complex electromagnetic environments.

4. Joint Jamming Avoidance and Suppression Anti-Jamming Wireless Transmission Technique

This section uses the detection results from Section 3 to guide resource allocation and jamming suppression. Resources with lower interference are selected for transmission, while detected jammed subcarriers are suppressed at the receiver.

4.1. Jamming Suppression Strategy Based on Intelligent FCME Algorithm

Based on the intelligent FCME jamming detection algorithm, the jamming frequency point set $\mathcal{J}$ is obtained, with amplitudes J_k, and the average power of jammed frequency points is:

$$\bar{P}_j = \frac{1}{|\mathcal{J}|} \sum_{k \in \mathcal{J}} |J_k|^2 \tag{15}$$

where $|\mathcal{J}|$ is the number of jammed frequency points. The unjammed frequency point set is $\mathcal{U}$, and the average signal power of unjammed portions is:

$$\bar{P}_s = \frac{1}{|\mathcal{U}|} \sum_{k \in \mathcal{U}} |Y_k|^2 \tag{16}$$

By scaling the signal, the scaled jammed subcarrier signal can be obtained as:

$$\tilde{y}_k = \lambda \frac{\bar{P}_s}{\bar{P}_j} \cdot y_k, \quad k \in \mathcal{J} \tag{17}$$

where λ is the scaling factor. A larger value retains more residual jamming, while a smaller value removes more useful signal information.

4.2. Jamming Avoidance Strategy Based on Type 0

Based on the intelligent FCME detection results, the system estimates IPN and user-received signal power to support Type 0 resource allocation. The IPN values describe the interference and noise level across the available frequency resources. The system gives priority to RBGs with lower IPN and uses the estimated user signal power to evaluate the transmission quality of the selected resources. It then selects the MCS and checks whether the supported data amount meets the user's request. In this way, the allocation process considers both jamming conditions and user requirements when assigning frequency resources.

Algorithm 2 presents the proposed anti-jamming time-frequency resource allocation algorithm. To simplify calculations, RB-level IPN is converted to RBG-level IPN, which provides certain resource allocation granularity during scheduling, enabling resource allocation to meet different service requirements while ensuring certain flexibility and efficiency. Based on the above allocation principles, the IPN of the g-th RBG is

$$P_{\mathrm{IPN},g} = \frac{1}{N_{\mathrm{RB}}^{\mathrm{RBG}}} \sum_{m \in \mathcal{G}_g} P_{\mathrm{IPN},m} \tag{18}$$

where $N_{\mathrm{RB}}^{\mathrm{RBG}}$ represents the number of RBs in each RBG. Next, all RBGs are sorted in ascending order according to IPN values

$$P_{\mathrm{IPN},(1)} \leq P_{\mathrm{IPN},(2)} \leq \cdots \leq P_{\mathrm{IPN},(G)} \tag{19}$$

User u selects RBGs in order and calculates SINR through user-received signal power P_u and the IPN of the currently selected RBG

$$\gamma_u = \frac{P_u}{\sum_{g \in \mathcal{G}_u} P_{\mathrm{IPN},g}} \tag{20}$$

where $\sum_{g \in \mathcal{G}_u} P_{\mathrm{IPN},g}$ is the sum of IPN of currently selected RBGs. If γ_u is greater than the SINR threshold γ_{th}, the newly added RBG at the current moment is retained, and the MCS obtained from table lookup based on SINR value and spectral efficiency φ are used to calculate transmittable data amount

$$D_{\mathrm{curr}} = \varphi \cdot B_u \cdot T_s \tag{21}$$

where B_u is the bandwidth occupied by currently selected RBGs and T_s represents symbol time. If D_{curr} is greater than the transmittable data amount calculated in the previous RBG selection loop, the newly added RBG is retained for the current user, and the next RBG continues to be selected. Repeat the above process until γ_u does not satisfy the condition or user u's requested data amount D_u is met. The total transmittable data amount for user u is:

$$D_u = \sum_{g \in \mathcal{G}_u} \varphi_g \cdot B_g \cdot T_s \tag{22}$$

Algorithm 2 Jamming avoidance algorithm based on Type 0

Input IPN of each RBG $\mathbf{P}_{\text{IPN}}$, signal-to-interference-plus-noise ratio (SINR) threshold γ_{th}, ordered user list $\mathcal{U}$, user power $\{P_u\}$, user requested data amount $\{D_u\}$
Output RBG allocation matrix $\mathbf{X}$, MCS and transport block size TBSize for each user

Initialize $\mathbf{X} = \mathbf{0}$, all TBSize $= 0$, and all MCS values as unassigned
Sort RBGs by ascending IPN to obtain the available list $\mathcal{L}$
while $\mathcal{U} \neq \emptyset$ **and** $\mathcal{L} \neq \emptyset$ **do**
    Select the first user u in $\mathcal{U}$
    Initialize $\mathcal{M}_u = \emptyset$ and $D_{\text{prev}} = 0$
    while $\mathcal{L} \neq \emptyset$ **and** $D_{\text{prev}} < D_u$ **do**
        Select the first RBG m in $\mathcal{L}$
        $\mathcal{M}_u = \mathcal{M}_u \cup \{m\}$
        Calculate $\gamma_u = P_u / \sum_{g \in \mathcal{M}_u} P_{\text{IPN},g}$
        if $\gamma_u < \gamma_{\text{th}}$ **then**
            $\mathcal{M}_u = \mathcal{M}_u \setminus \{m\}$
            break
        end if
        Look up the candidate MCS and its spectral efficiency φ
        Calculate $D_{\text{curr}} = \varphi B_u T_s$ for the candidate set
        if $D_{\text{curr}} \leq D_{\text{prev}}$ **then**
            $\mathcal{M}_u = \mathcal{M}_u \setminus \{m\}$
            break
        end if
        Accept the candidate MCS and set $D_{\text{prev}} = D_{\text{curr}}$
        Remove m from $\mathcal{L}$
    end while
    Set $x_{g,u} = 1$ for all $g \in \mathcal{M}_u$ and $\text{TBSize}_u = D_{\text{prev}}$
    Remove user u from $\mathcal{U}$
end while

After current user selection completes, the algorithm continues allocating RBGs for subsequent users until all user-requested data amounts are satisfied or RBG resources are exhausted. The optimization objective of this algorithm is to maximize system sum rate under jamming conditions:

$$\max_{\mathbf{X}} \sum_{u \in \mathcal{U}} R_u \tag{23}$$

subject to constraints:

$$\sum_{u \in \mathcal{U}} x_{g,u} \leq 1, \quad \forall g \tag{24}$$

where $x_{g,u}$ is a binary variable indicating whether the g-th RBG is allocated to user u. Through the above steps, the time-frequency resource allocation algorithm can efficiently allocate spectrum resources and improve system performance.

4.3. Overall Process of Joint Jamming Avoidance and Suppression Anti-Jamming Algorithm

Figure 2 shows the overall process of the proposed JJAS method. Jamming-type information can be provided by existing recognition methods [30,31]. When continuous band jamming is detected, using jamming suppression alone significantly reduces MCS, causing transmission rates to drop sharply. Therefore, the system first adopts the jamming avoidance mechanism, switching to unjammed or weakly jammed frequency bands for communication to ensure communication link continuity. Meanwhile, to avoid inaccurate jamming detection results from previous time slots, jamming suppression strategy is adopted during data reception to reduce jamming effects on data transmission.

If comb-spectrum jamming is detected, the system only adopts the jamming suppression algorithm without using jamming avoidance. This is because comb-spectrum jamming

characteristics involve generating jamming signals at multiple discrete frequency points, with each jamming portion occupying relatively small bandwidth, making it difficult to find large amounts of continuous unjammed frequency bands, and jamming does not cover the entire communication frequency band. Therefore, the system can still transmit data with lower MCS. By reducing MCS, communication link stability can be maintained in jamming environments.

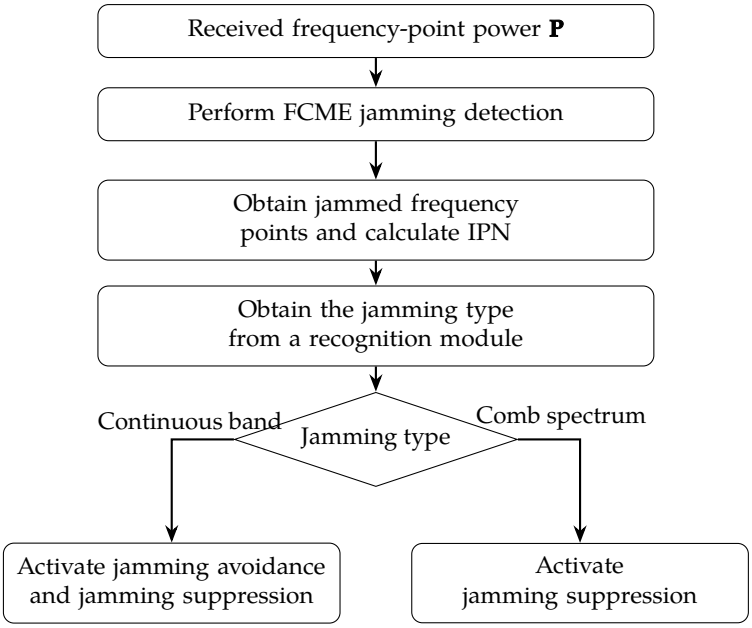


Figure 2. Flowchart of the JJAS method.

4.4. Computational Complexity and System Overhead

For the N frequency points in Algorithm 1, sorting costs $O(N \log N)$, and each outer iteration costs $O(N)$ for mean-power calculation and candidate checks. Each successful iteration removes at least one candidate, so the FCME procedure has a worst-case cost of $O(N^2)$ including sorting. Subcarrier suppression costs $O(N)$. In Algorithm 2, sorting the G RBGs costs $O(G \log G)$. Algorithm 2 removes accepted RBGs from the available list and moves to the next user when a candidate is rejected or the demand is met. Each user therefore checks each RBG at most once. Recomputing the IPN sum for each candidate set gives an allocation cost of at most $O(|\mathcal{U}|G^2)$, using the initial user set $\mathcal{U}$.

Compared with conventional transmission, the proposed scheme adds the IPN/signal power and jamming detection and suppression modules shown in Figure 1 and modifies the resource allocation module. The IPN/signal power module uses the detection results to estimate IPN power and user signal power. This requires power calculations and averaging, together with storage of the estimates. The detection and suppression module requires FCME sorting and threshold checks, followed by scaling of the detected jammed subcarriers. Adaptive threshold selection also requires the Q-table and its updates. The modified resource allocation module retains Type 0 RBG allocation and MCS lookup but uses the detection-based power estimates to evaluate candidate RBGs. Its cost therefore includes RBG sorting, SINR calculation, and MCS lookup.

5. Simulation Analysis

In this paper, simulation experiments adopt a Sub-6G typical scenario with the following configuration: OFDM subcarrier spacing Δf is 30 kHz, the half-frame duration is 5 ms and contains ten slots of 0.5 ms each, including two downlink slots, one special slot, and seven uplink slots. The available MCS indices are 0 to 27, covering quadrature phase shift

keying (QPSK) and 16-, 64-, and 256-point quadrature amplitude modulation (QAM). The specific simulation system parameter configuration is shown in Table 1.

Table 1. Simulation system parameter configuration.

Parameter	Value
Center frequency	3.3 GHz
User bandwidth	100 MHz
Transmit/Receive antenna gain	19 dBi
User transmit power	43 dBm
Jamming type	Comb-spectrum jamming, continuous-band jamming
Number of users	4
Scaling factor	0
Number of RBGs	17
User data request amount	1500 bytes/slot
BER threshold	0.1
SINR threshold	−4.7 dB
Sum rate reward weight	0.1
BER penalty weight	0.5
Low sum rate threshold	18 Mbps
Medium sum rate threshold	32 Mbps
Low BER threshold	0.1
Medium BER threshold	0.5
Initial Q value	0
Learning rate α_Q	0.01
Discount factor γ	0.9
Exploration probability ϵ	0.3
Run length	200 time slots

First, continuous band jamming occupying 30% of bandwidth as shown in Figure 3 is applied to interfere with the Sub-6G communication uplink. Figure 4 shows the comparison of jamming detection accuracy and BER between the proposed FCME-based intelligent jamming detection algorithm and traditional fixed threshold FCME jamming detection algorithm under continuous band jamming scenarios. In the initial stage, due to lack of prior information, the proposed FCME-based intelligent jamming detection algorithm undergoes approximately 20 time slots to learn the optimal jamming threshold factor. During this process, the BER exhibits fluctuating states, and jamming detection accuracy is close to zero. As the learning stage completes, the BER approaches zero, and jamming detection accuracy reaches nearly 100% in most time slots. At the 100-th time slot, jamming changes, with JSR decreasing from 10 dB to 2 dB, causing jamming detection accuracy fluctuations and instantaneous BER increases. After approximately 20 time slots of relearning, the model acquires the new optimal threshold factor, the BER subsequently decreases and stabilizes, and jamming detection accuracy improves accordingly. This fully demonstrates that the algorithm possesses good adaptation and self-learning capabilities for jamming variation scenarios.

In the traditional FCME jamming detection algorithm, the jamming threshold factor is fixed at 0.8. As shown in Figure 4, the fixed-threshold FCME jamming detection algorithm performs well in the first 100 time slots. However, after 100 time slots, when jamming changes, jamming detection accuracy drops to approximately zero, BERs fluctuate, and the algorithm cannot automatically adjust to adapt to new situations. System performance continuously deteriorates due to jamming changes, making it difficult to guarantee communication quality in dynamic jamming environments.

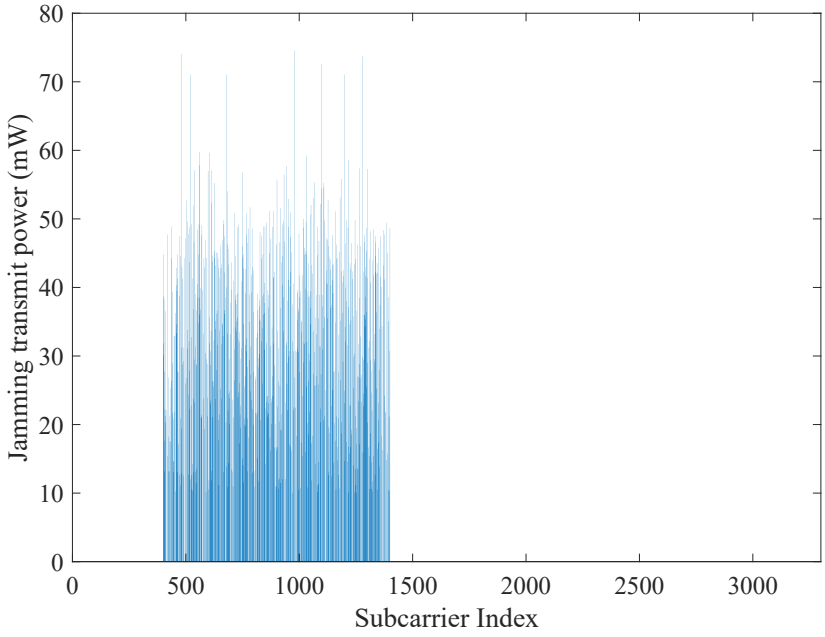


Figure 3. Continuous band jamming schematic diagram.

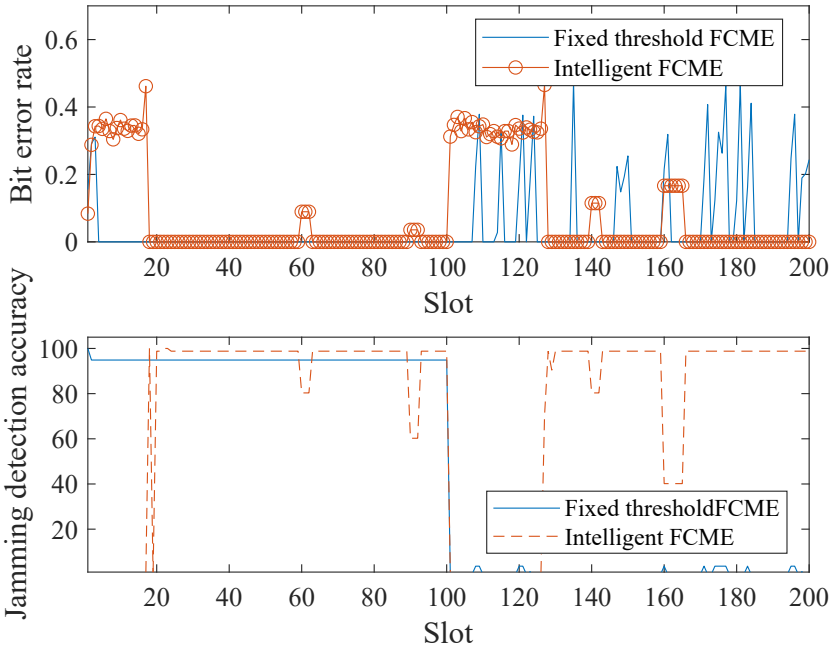


Figure 4. Comparison of jamming detection accuracy and BER between intelligent FCME algorithm and fixed threshold FCME algorithm under continuous band jamming.

Under continuous band jamming scenarios, with received JSR set to 35 dB, performance comparison is conducted between the proposed JJAS algorithm and traditional Type 0 resource allocation algorithm. Figure 5 shows RBG allocation under different resource allocation strategies. It can be observed that the JJAS algorithm performs accurate resource allocation based on continuous band jamming conditions and user requirements from the initial stage, avoiding the use of jammed RBG frequency bands in subsequent time slots. Traditional Type 0 resource allocation methods have estimation deviations for continuous band jamming, leading to inaccurate calculations of key parameters such as IPN and user power. These inaccuracies extend to the resource allocation stage, causing the algorithm

to make mistakes when evaluating unjammed frequency bands, ultimately resulting in insufficient and unreasonable resource utilization and unnecessary resource waste.

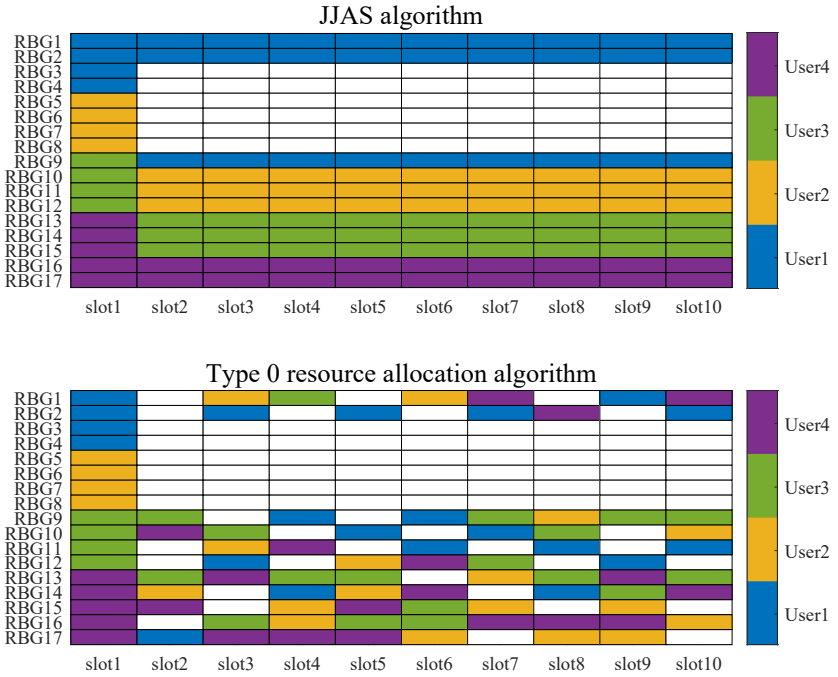


Figure 5. Comparison of RBG allocation between JJAS algorithm and traditional Type 0 resource allocation algorithm under continuous band jamming scenarios.

Figure 6 shows the transmission rate of the proposed JJAS algorithm and the Type 0 resource allocation algorithm. It can be found that the proposed JJAS algorithm achieves accurate estimation of user power and IPN, thereby enabling accurate MCS and RBG allocation, and consequently achieving higher user data transmission rates. Traditional Type 0 resource allocation algorithms are affected by continuous band jamming, resulting in deviations during channel estimation, which subsequently leads to inaccurate IPN estimation. These inaccuracies prevent resource allocation from reaching optimal states, ultimately resulting in lower user rates.

The comb-spectrum jamming components are placed within a frequency interval covering 40% of the total subcarrier range. Seven components, each occupying 20 subcarriers, jam 140 of the 3276 subcarriers, giving an actual occupied fraction of about 4.27%. As shown in Figure 7, the jamming is applied to the Sub-6G uplink with a received JSR of 35 dB. The first component starts at subcarrier 401, and the starting positions of adjacent components are separated by 200 subcarriers.

Figure 8 shows the RBG allocation comparison between the proposed JJAS algorithm and traditional Type 0 resource allocation algorithm under comb-spectrum jamming scenarios. When using the JJAS algorithm, the system implements jamming suppression strategies for jammed frequency bands. Under this strategy, users can maintain communication link operation on jammed RBGs by reducing MCS levels. It can be found that all RBGs are effectively allocated to users, fully demonstrating the algorithm's capability to efficiently utilize limited RBG resources and maintain communication link operation and user communication needs in jamming environments. Traditional Type-0 resource allocation algorithms cannot accurately estimate the IPN level, making reliable communication on jammed RBGs extremely difficult. Therefore, during actual resource allocation, this algorithm chooses not to use jammed RBGs, exhibiting limitations in dynamic adjustment capabilities for RBG resources.

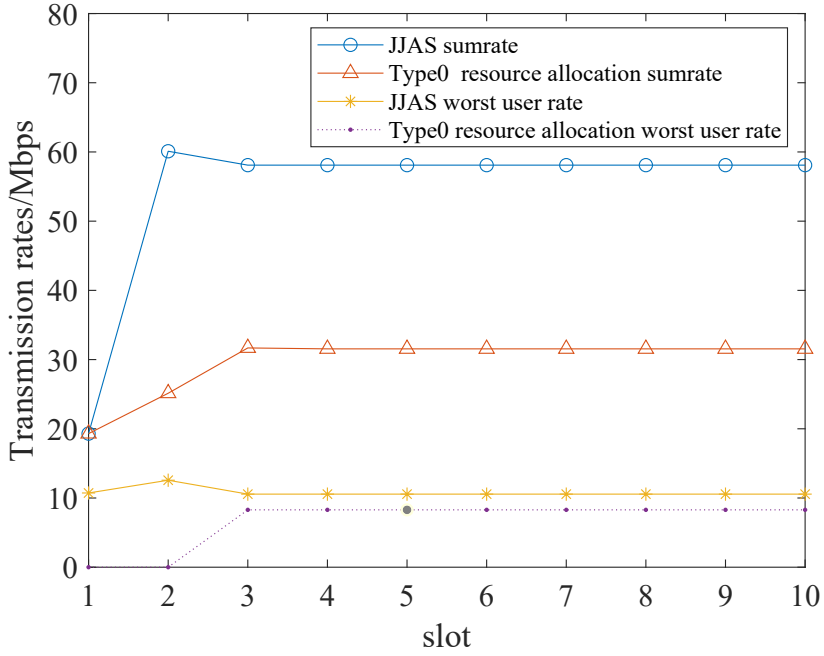


Figure 6. Comparison of user rates between JJAS algorithm and traditional Type 0 resource allocation algorithm under continuous band jamming scenarios.

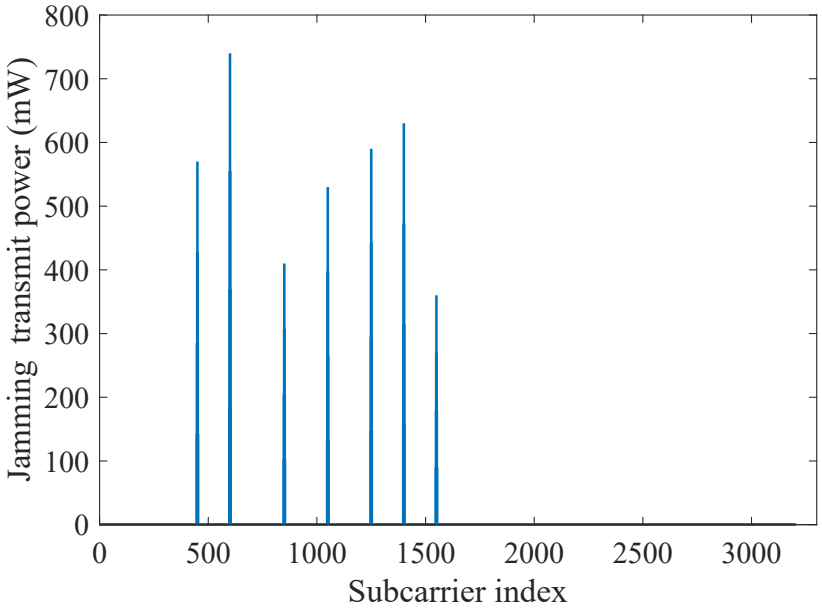


Figure 7. Comb-spectrum jamming schematic diagram.

Figure 9 compares the sum rate and worst-user rate of the two algorithms under comb-spectrum jamming. The sum rate of JJAS stays at about 60 Mbps across the time slots, while that of the Type 0 resource allocation algorithm stays at about 30 Mbps. JJAS also maintains a worst-user rate of about 10 Mbps, whereas the Type 0 algorithm gives a much lower rate. These results are consistent with the RBG allocation in Figure 8. JJAS uses lower MCS levels to support transmission on jammed RBGs. The Type 0 algorithm leaves these RBGs unused because of inaccurate IPN estimation, reducing the resources available for data transmission.

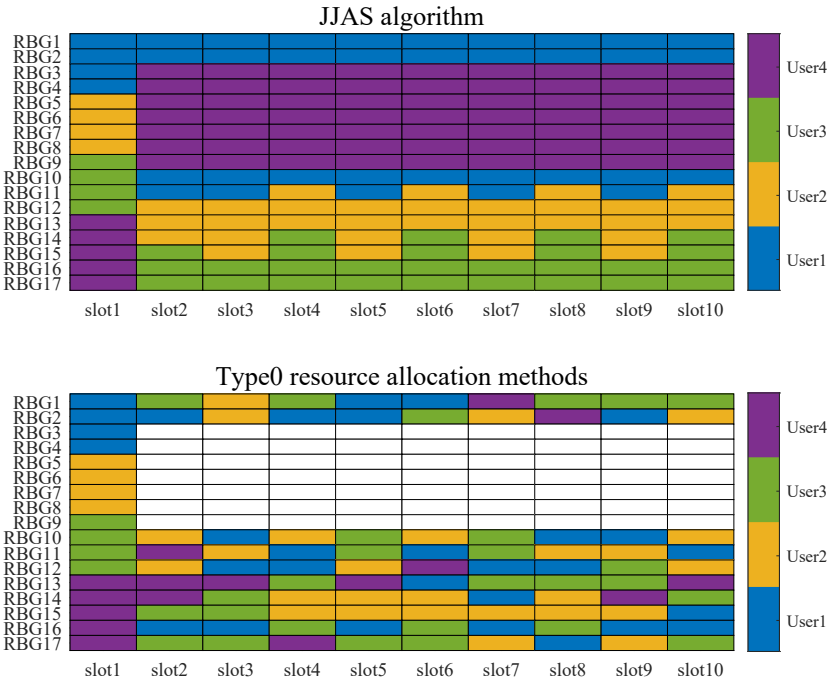


Figure 8. Comparison of RBG allocation between JJAS algorithm and traditional Type 0 resource allocation algorithm under comb-spectrum jamming scenarios.

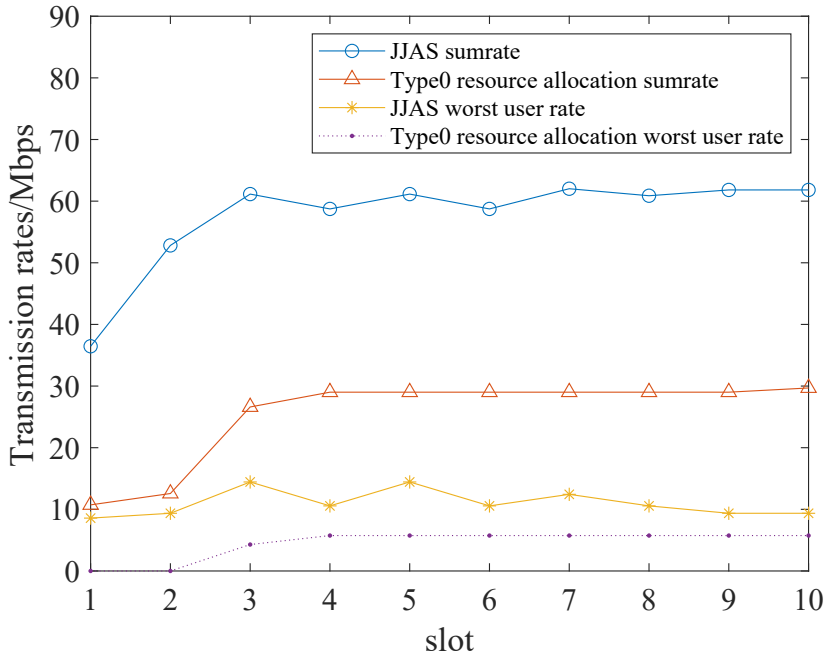


Figure 9. Comparison of user rates between JJAS algorithm and traditional Type 0 resource allocation algorithm under comb-spectrum jamming scenarios.

6. Conclusions

This paper focuses on communication reliability issues in complex electromagnetic jamming environments and proposes an anti-jamming wireless transmission technique integrating time-frequency domain jamming avoidance and suppression mechanisms for dynamic jamming environments, with particular relevance to emergency communication scenarios. Through constructing a Q-learning-based FCME jamming detection framework, dynamic adaptive optimization of jamming detection threshold factors is achieved. This

mechanism breaks through the limitations of traditional fixed jamming thresholds, enabling real-time perception of dynamic changes in jamming environments. Under complex scenarios such as jamming intensity variations and frequency hopping, precise detection of jamming signals is achieved, effectively improving jamming detection accuracy and response speed. Based on IPN parameters, user power distribution, and other key information obtained from jamming detection, the JJAS algorithm is innovatively designed. Experimental results demonstrate that this scheme significantly improves system anti-jamming robustness while guaranteeing system sum rates, providing new technical paths and theoretical support for solving communication reliability issues in complex electromagnetic environments, and supporting resilient emergency communications.

Actual electromagnetic environments contain complex factors such as multi-source jamming superposition and signal propagation multipath effects, which differ significantly from simulation environments. Future research should conduct large-scale real-scenario testing to validate algorithm effectiveness and stability in real complex electromagnetic environments, especially in infrastructure-impaired emergency communication settings.

Author Contributions: Writing—original draft, Z.L.; software, Z.L., L.Z. and L.H.; writing—review and editing, Z.L., L.H., Z.Z. and C.Z. (Changwei Zhang); formal analysis, L.Z. and X.W.; visualization, L.Z.; investigation, L.Z.; data curation, X.W.; validation, Z.Z.; supervision, C.Z. (Cheng Zhang); project administration, C.Z. (Cheng Zhang) and C.Z. (Changwei Zhang); conceptualization, C.Z. (Changwei Zhang); funding acquisition, C.Z. (Changwei Zhang). All authors have read and agreed to the published version of the manuscript.

Funding: This work was supported in part by the National Natural Science Foundation of China under Grant 62401641, and in part by CRSC Low-Altitude Intelligence Technology Co., Ltd. under Grant 6800-K1240008.

Data Availability Statement: Data will be made available on request.

Conflicts of Interest: Authors Zhiyu Li, Xiaoyang Wang, and Lili Hu were employed by the company CRSC Low-Altitude Intelligence Technology Co., Ltd. The remaining authors declare that the research was conducted in the absence of any commercial or financial relationships that could be construed as a potential conflict of interest.

References

1. Giordani, M.; Polese, M.; Mezzavilla, M.; Rangan, S.; Zorzi, M. Toward 6G networks: Use cases and technologies. *IEEE Commun. Mag.* **2020**, *58*, 55–61. [CrossRef]
2. Rappaport, T.S.; Xing, Y.; Kanhere, O.; Ju, S.; Madanayake, A.; Mandal, S. Wireless communications and applications above 100 GHz: Opportunities and challenges for 6G and beyond. *IEEE Access* **2019**, *7*, 78729–78757. [CrossRef]
3. Saad, W.; Bennis, M.; Chen, M. A vision of 6G wireless systems: Applications, trends, technologies, and open research problems. *IEEE Netw.* **2020**, *34*, 134–142. [CrossRef]
4. Yi, W.; Varshney, P.K. Adaptation of frequency hopping interval for radar anti-jamming based on reinforcement learning. *IEEE Trans. Veh. Technol.* **2022**, *71*, 12434–12449. [CrossRef]
5. Xu, Y.; Chen, J.; Xu, Y.; Gu, F.; Yao, K.; Jia, L. Energy-efficient channel access and data offloading against dynamic jamming attacks. *IEEE Trans. Green Commun. Netw.* **2021**, *5*, 1734–1746. [CrossRef]
6. Zhang, H.; Xu, M.; Liu, W.; Zhang, Q.; Zhang, L.; Xu, H. Dwell time allocation in a PAR network for maneuvering target tracking under clutter environment. *Chin. J. Aeronaut.* **2026**, 104370. [CrossRef]
7. Zhang, H.; Liu, W.; Shi, J.; Fei, T.; Zong, B. Joint detection threshold optimization and illumination time allocation strategy for cognitive tracking in a networked radar system. *IEEE Trans. Signal Process.* **2022**, *70*, 5833–5847. [CrossRef]
8. Vartiainen, J.; Vuohtoniemi, R. False alarm rate analysis of the FCME algorithm in cognitive radio applications. In Proceedings of the 2015 Advanced International Conference on Telecommunications (AICT 2015), Brussels, Belgium, 21–26 June 2015; pp. 102–106.
9. Zhou, H.; Dong, C.; Wu, R.; Xu, X.; Guo, Z. Feature fusion based on Bayesian decision theory for radar deception jamming recognition. *IEEE Access* **2021**, *9*, 16296–16304. [CrossRef]

10. Saarnisaari, H.; Henttu, P. Impulse detection and rejection methods for radio systems. In Proceedings of the 2003 IEEE Military Communications Conference (MILCOM), Boston, MA, USA, 13–16 October 2003; pp. 1126–1131.
11. Zhang, C.; Xue, L.; Zhang, E. Narrow-band interference suppression in transform domain based on an adaptive multi-threshold algorithm. *J. Electron. Inf. Technol.* **2006**, *28*, 461–465.
12. Lehtomaki, J.J.; Vartiainen, J.; Juntti, M.; Saarnisaari, H. Analysis of the LAD methods. *IEEE Signal Process. Lett.* **2008**, *15*, 237–240. [CrossRef]
13. Wang, C.; Chen, Y.; Lin, Z.; Chen, Q.; Xiao, L. Reinforcement learning based jamming detection for reliable wireless communications. In Proceedings of the 2024 IEEE 99th Vehicular Technology Conference (VTC2024-Spring), Singapore, 24–27 June 2024; pp. 1–2.
14. Li, Y.; Xu, Y.; Li, G.; Gong, Y.; Liu, X.; Wang, H. Dynamic spectrum anti-jamming access with fast convergence: A labeled deep reinforcement learning approach. *IEEE Trans. Inf. Forensics Secur.* **2023**, *18*, 5447–5458. [CrossRef]
15. Qi, N.; Wang, W.; Xiao, M.; Jia, L.; Jin, S.; Zhu, Q. A learning-based spectrum access Stackelberg game: Friendly jammer-assisted communication confrontation. *IEEE Trans. Veh. Technol.* **2021**, *70*, 700–713. [CrossRef]
16. Chen, M.; Liu, W.; Zhang, N.; Li, J.; Ren, Y.; Yi, M.; Liu, A. GPDS: A multi-agent deep reinforcement learning game for anti-jamming secure computing in MEC network. *Expert Syst. Appl.* **2022**, *210*, 118394. [CrossRef]
17. Atheeq, C.; Gulzar, Z.; Al Reshan, M.S.; Alshahrani, H.; Sulaiman, A.; Shaikh, A. Securing UAV networks: A lightweight chaotic-frequency hopping approach to counter jamming attacks. *IEEE Access* **2024**, *12*, 38685–38699. [CrossRef]
18. Cheng, S.; Ling, X.; Zhu, L. Deep reinforcement learning-based anti-jamming approach for fast frequency hopping systems. *IEEE Open J. Commun. Soc.* **2025**, *6*, 961–971. [CrossRef]
19. Shi, Y.; An, K.; Li, Y. Index modulation based frequency hopping: Anti-jamming design and analysis. *IEEE Trans. Veh. Technol.* **2021**, *70*, 6930–6942. [CrossRef]
20. Fonteneau, C.; Crussière, M.; Bazin, A.; Pasquero, O.P. Rejection capability of anti-jamming Wiener filter for multi-tone interference in DSSS systems. In Proceedings of the 2024 IEEE Military Communications Conference (MILCOM), Washington, DC, USA, 8 October 2024–1 November 2024; pp. 1–6.
21. Qi, J.; Zhang, H.; Qi, X.; Peng, M. Deep reinforcement learning based hopping strategy for wideband anti-jamming wireless communications. *IEEE Trans. Veh. Technol.* **2024**, *73*, 3568–3579. [CrossRef]
22. Dutta, T.; Satija, U.; Ramkumar, B.; Manikandan, M.S. Blind impulse estimation and removal using sparse signal decomposition framework for OFDM systems. *Circuits Syst. Signal Process.* **2018**, *37*, 847–861. [CrossRef]
23. Shhabi, L.; Rizaner, A.; Ulusoy, A.H.; Amca, H. Suppressing the effect of impulsive noise on millimeter-wave communications systems. *Radioengineering* **2020**, *29*, 376–385. [CrossRef]
24. Liu, Y.; Zhang, B.; Guo, D.; Wang, H.; Ding, G.; Yang, N. A game theoretical anti-jamming beamforming approach for integrated sensing and communications systems. *IEEE Trans. Veh. Technol.* **2024**, *73*, 15780–15785. [CrossRef]
25. Qi, X.; Peng, M.; Zhang, H.; Kong, X. Anti-jamming hybrid beamforming design for millimeter-wave massive MIMO systems. *IEEE Trans. Wirel. Commun.* **2024**, *23*, 9160–9172. [CrossRef]
26. Wang, Z.; Zhang, C.; Zhang, C.; Huang, Y. Anti-jamming transmission of downlink cell free millimeter-wave MIMO system. *IEEE Wirel. Commun. Lett.* **2025**, *14*, 954–958. [CrossRef]
27. Hao, C.; Sun, X. Adaptive anti-jamming beamforming based on the preprocessing deep reinforcement learning for downlink navigation communication. *J. Ambient Intell. Humaniz. Comput.* **2023**, *14*, 14057–14069. [CrossRef]
28. Hou, Z.; Chen, J.; Huang, Y.; Luo, Y.; Wang, X.; Gu, J. Joint trajectory and passive beamforming optimization in IRS-UAV enhanced anti-jamming communication networks. *China Commun.* **2022**, *19*, 191–205. [CrossRef]
29. Capozzi, F.; Piro, G.; Grieco, L.A.; Boggia, G.; Camarda, P. Downlink packet scheduling in LTE cellular networks: Key design issues and a survey. *IEEE Commun. Surv. Tutor.* **2013**, *15*, 678–700. [CrossRef]
30. Ge, R.; Li, Y.; Zhu, Y.; Zhang, X.; Zhang, K.; Chen, M. Method for recognition of communication interference signals under small-sample conditions. *Appl. Sci.* **2024**, *14*, 5869. [CrossRef]
31. Zhang, N.; Li, Y.; Shi, Y.; Shen, J. A CNN-based adaptive federated learning approach for communication jamming recognition. *Electronics* **2023**, *12*, 3425. [CrossRef]

Disclaimer/Publisher's Note: The statements, opinions and data contained in all publications are solely those of the individual author(s) and contributor(s) and not of MDPI and/or the editor(s). MDPI and/or the editor(s) disclaim responsibility for any injury to people or property resulting from any ideas, methods, instructions or products referred to in the content.